EMITTANCE GROWTH SCALING LAWS IN RESONANCE CROSSING*

X. Pang, F. Wang, X. Wang, S.Y. Lee, Dept. of Phys., Indiana University, IN 47405, USA
K.Y. Ng, FNAL, P.O. Box 500, Batavia, IL 60510, USA

Abstract

Scaling laws of the emittance growth factor (EGF) for a beam crossing the 6th order systematic space-charge resonances and the random 4th order resonance driven by octupoles are obtained by numerical multi-particle simulations. These scaling laws can be used in setting the minimum acceleration rate, and the maximum tolerable resonance strength for the design of non-scaling fixed-field alternating gradient (FFAG) accelerators.

INTRODUCTION

The discovery of strong focusing principle [1] in the 1950's revolutionized the design of high energy accelerators and led to the construction of the Alternating Gradient Synchrotron (AGS) in the Brookhaven National Laboratory. Based on the strong focusing principle, the Midwest University Research Association (MURA) proposed the concept of the Fixed-field alternating gradient accelerators (FFAGs) in the 1950's [2], but the community favored a higher energy accelerator and constructed the zero-gradient-synchrotron (ZGS) in Argonne National Laboratory. Recently the FFAG idea has been revived as high beam-power is in demand. The beam pulse repetition rate in an accelerator is essentially determined by the ramping rate of the pulsed magnetic guide-field and the achievable accelerating voltage in rf cavities. The FFAGs have an advantage over conventional synchrotrons owing to the fact that the guide-field is constant so that the repetition rate can be made considerably higher up to kHz.

Nonlinear resonances are important to all strong focusing accelerators. The betatron and synchrotron tunes are thus maintained constant in order to avoid major resonances. The FFAG accelerators that maintain constant betatron tunes during the accelerating cycle require a large magnet aperture with high nonlinear magnetic fields. For example, the 150-MeV FFAG in Japan has a radial beam excursion from 4.4 to 5.3 m in an accelerating cycle from 12 MeV to 150 MeV, where the betatron tunes are $\nu_x \in (3.69, 3.80)$ and $\nu_z \in (1.14, 1.30)$ [3]. The design that keeps the betatron tunes nearly constant is called the *scaling* FFAG accelerators

To overcome the complexity and the size of the FFAG magnets, the betatron tunes are left to vary as the beam energy increases. Such designs are called *non-scaling* FFAGs [4]. The non-scaling design has been considered as a favorable candidate for the acceleration of the muon beams, where the tune ramp rate can be high because of its small rest mass. Recently, the non-scaling FFAG has been considered as proton drivers for neutrino factories, muon colliders, and other applications. For example, Ruggiero suggested to use three concentric FFAGs as a proton driver to replace the Brookhaven AGS [5] for reaching a final beam power of more than 10 MW. For each FFAG, the beam closed orbit has a radial excursion of less than 18 cm during the acceleration cycle. The betatron tunes vary from $\nu_{x,z} = (40.0, 38.1)$ to (19.1, 9.3) during acceleration. As shown in Fig. 1, the ramping cycle will cross both the systematic 4th and 6th order resonances, $4\nu_x = P$, $4\nu_z = P$, $2\nu_x + 2\nu_z = P$, $6\nu_x = P$, $6\nu_z = P$, $4\nu_x + 2\nu_z = P$, and $2\nu_x + 4\nu_z = P$, where $P = 136$ is the periodicity of the lattice.

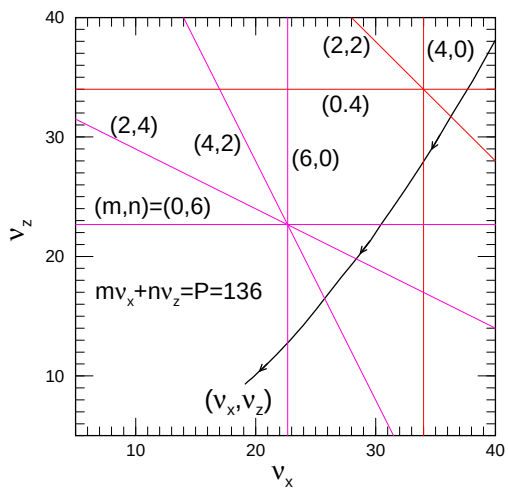

Figure 1: Tune diagram of FFAGs proposed by Ruggiero [5] to replace the Brookhaven AGS. Notice that the tunes of the FFAGs ramp from $(\nu_x, \nu_z) = (40.0,\ 38.1)$ to (19.2, 9.3) crossing the systematic 4th and 6th order resonances.

For the proton driver in the non-scaling FFAG design, the betatron tune-ramp rate is approximately given by

$$\frac{\Delta\nu_{x,z}}{\Delta n} \sim -\frac{\nu_{x,z}}{\beta^2 E}\frac{\Delta E}{\Delta n}, \qquad (1)$$

where β is the relativistic velocity factor, ν_x and ν_z are the horizontal and vertical betatron tunes, E is the beam energy, and $\Delta E/\Delta n$ is the energy gain per revolution, which depends essentially on the achievable rf voltage in the rf cavities. During the acceleration cycle, the beam motion encounters many resonances. The beam quality is an important issue as systematic and random resonances are crossed.

*Work supported by US Department of Energy under contracts DE-FG0292ER40747,DEAC02-76CH03000, and National Science Foundation NSF PHY-0552389.

Recently, Lee pointed out that the systematic nonlinear resonances driven by the self space-charge force may cause substantial emittance growth when the resonances are crossed [6]. He demonstrated a simple scaling property for the emittance growth across the 4th order space-charge resonance. A later article by Lee *et al.* shows that parametric linear and nonlinear resonances driven by random field errors, although correctable, can also lead to emittance growth depending on how fast these resonances are crossed [7].

The emittance growth of sextupolar resonances have been studied in the past [8]. This paper will investigate the emittance growth when crossing the systematic 6th order resonances and the parametric 4th order resonances driven by random nonlinear magnetic fields. We would like to establish scaling laws for these resonances. Given a space-charge tune shift and a resonance strength, we wish to obtain the minimum resonance crossing rate so that emittance growth remains tolerable. In particular, unlike the approximation used in Refs. [6, 7], the space-charge force in a bi-Gaussian beam is used in this study.

THE MODEL

Our investigation bases mostly on multi-particle simulations. The accelerator lattice used in our study is made of 24 FODO cells, where each FODO cell is composed of a focusing quadrupole and a defocusing quadrupole separated by dipoles for completing a closed orbit for a synchrotron. Examples of synchrotrons made of FODO cells are the Fermilab Booster, the Alternating Gradient Synchrotron (AGS) in Brookhaven National Laboratory and the AGS Booster. The superperiodicity of our model is 24. Four-by-four transfer matrices are employed for each period from a D-magnet to the next F-magnet and from the F-magnet to next D-magnet, thus completing a FODO cell. Thus the betatron phase space coordinates are transported by the transfer matrices $M_{F\to D}(\beta_{x,\mathrm{D}}, \beta_{z,\mathrm{D}}, \beta_{x,\mathrm{F}}, \beta_{z,\mathrm{F}}, \psi_x, \psi_z)$, and $M_{D\to F}(\beta_{x,\mathrm{F}}, \beta_{z,\mathrm{F}}, \beta_{x,\mathrm{D}}, \beta_{z,\mathrm{D}}, \psi_x, \psi_z)$ [6, 7, 9]. Typical betatron functions are $\beta_{x,\mathrm{F}} = 40$ m, $\beta_{z,\mathrm{F}} = 8.3$ m, at the center of the focusing quadrupole and $\beta_{x,\mathrm{D}} = 6.3$ m, $\beta_{z,\mathrm{D}} = 21.4$ m at the center of the defocusing quadrupole. The dispersion functions are $D_{x,\mathrm{D}} = 2.54$ m and $D_{x,\mathrm{F}} = 4.5$ m at the mid-point between two D and two F magnets respectively. The betatron tunes will be varied according to the requirement of the simulations.

The transverse distribution is assumed to be bi-Gaussian all the time. At the end of each revolution turn, the transverse rms beam radii and the position of the beam center are computed from the multi-particle phase space distribution. The transverse rms emittances are obtained from each superperiod. The information is used to compute the space-charge force, which is applied at each F-magnet and D-magnet in the succeeding revolution turn. This procedure has the advantage that the noise in the calculation of the radii is smoothed out in one turn, so that the number of macro-particles, usually 2000, used in the simulation need not be too large. The Gaussian-distribution assumption is certainly not self-consistent. However, this assumption simplifies the space-charge force and speeds up the simulations tremendously.

Space-Charge Force

Since the emittance growth rate is usually much faster than a synchrotron period, this justifies the performance of only 2D simulation for a slice of the beam at the longitudinal bunch center. For a beam with linear particle density N and bi-Gaussian charge distribution

$$\rho(x,z) = \frac{Ne}{2\pi\sigma_x\sigma_z} e^{-x^2/2\sigma_x^2 - z^2/2\sigma_z^2}, \tag{2}$$

with $\sigma_{x,z}$ being the rms horizontal and vertical beam radii including contribution coming from momentum dispersion, the transverse 2D space-charge potential is

$$V_{sc}(x,z) = \frac{K_{sc}}{2}\int_0^\infty \frac{\exp\left[-\frac{x^2}{2\sigma_x^2+t} - \frac{z^2}{2\sigma_z^2+t}\right] - 1}{\sqrt{(2\sigma_x^2+t)(2\sigma_z^2+t)}}\, dt, \tag{3}$$

where

$$K_{sc} = \frac{2Nr_0}{\beta^2\gamma^3} \tag{4}$$

is the space-charge perveance, r_0 is the particle classical radius, and β and γ are the relativistic parameters. In the simulation, we set the bunch intensity with N_{B} particles and an rms bunch-length σ_s to obtain $N = N_{\mathrm{B}}/\sqrt{2\pi}\sigma_s$. The space-charge force on each particle is obtained by Hamilton's equation. Thus each beam particle passing through a length Δs experiences a space-charge kick

$$\begin{aligned}\frac{\Delta x'}{\Delta s} &= -\frac{\partial V_{sc}}{\partial x} = F_{x,sc},\\ \frac{\Delta z'}{\Delta s} &= -\frac{\partial V_{sc}}{\partial z} = F_{z,sc}.\end{aligned} \tag{5}$$

It is straightforward to demonstrate that $F_{x,sc}$ and $F_{z,sc}$ can be expressed analytically in terms of the complex error function. Unfortunately, the application of the analytic expression is cumbersome, because it exhibits an apparent singularity when $\sigma_x = \sigma_z$. We have found out a way to avoid the singularity and other divergence of the analytic expression.

We expand the space-charge potential in Taylor series in order to study the systematic space charge resonances:

$$\begin{aligned}V_{sc}(x,z) = -\frac{K_{sc}}{2}\Bigg\{&\left[\frac{x^2}{\sigma_x(\sigma_x+\sigma_z)} + \frac{z^2}{\sigma_z(\sigma_x+\sigma_z)}\right]\\ &-\frac{1}{4\sigma_x^2(\sigma_x+\sigma_z)^2}\left[\frac{2+r}{3}x^4 + \frac{2}{r}x^2z^2 + \frac{1+2r}{3r^3}z^4\right]\\ &+\frac{1}{72\sigma_x^3(\sigma_x+\sigma_z)^3}\left[\frac{8+9r+3r^2}{5}x^6 + \frac{3(3+r)}{r}x^4z^2\right.\\ &\left.+\frac{3(3r+1)}{r^3}x^2z^4 + +\frac{8r^2+9r+3}{5r^5}z^6\right] + \cdots\Bigg\},\end{aligned} \tag{6}$$

with $r = \sigma_z/\sigma_x$. The first term inside the curly brackets represents the linear force, which gives rise to linear space charge tune shift. The second and the third terms drive the 4th and 6th order resonances. It is not possible, however, to truncate the expansion just up to the order of resonances that we wish to study. This is because the truncated space-charge force is accurate only for particles close the beam center and it will increase without limit for particles far away. However, results of our simulation show that the emittance growth in crossing a systematic resonance depends essentially on the harmonic content of one of the Taylor series terms.

SYSTEMATIC 6TH ORDER RESONANCE

If we inject protons at the rate of 4×10^{11} protons per turn, 100-turn injection implies 4×10^{13} particles in the accelerator. The parameters of our simulation model are set at harmonic number $h = 84$, circumference $C = 474.2$ m, and the bunching factor $B = C/(h\sqrt{2\pi}\sigma_s) = 2.0$. Actually, the space charge effect essentially depends on the parameter $BN_{\rm B}$ or on the maximum linear space-charge tune shifts, but not on $N_{\rm B}$ and B separately. The injected protons are bi-Gaussian distributed with initial horizontal and vertical normalized rms emittances of $\epsilon_{\rm N,rms} = 8.33\times10^{-6}$ πm or simply 8.33 μm. To study the systematic space charge resonances for an accelerator with 24 superperiods, the betatron tunes must cross $\nu_x = 4$ and $\nu_z = 4$. We choose the initial bare betatron tunes as $\nu_{x0} = 4.25$ and $\nu_{z0} = 4.45$. Since we are interested only in emittance increase in crossing the resonance, the kinetic energy of the beam particles is kept constant at 1 GeV during the tracking, while the betatron tunes are allowed to ramp starting from some specific turn according to some specific ramping rate so that they become $\nu_{x0} = 3.69$ and $\nu_{z0} = 3.89$ at turn 1600. The emittances at turn 1600 are read and are divided by the initial emittances to give the *emittance growth factors* (EGFs). Since we study the effects of the space-charge driven systematic resonances, all random fields errors and nonlinear fields in the magnets are turned off.

Resonance Strengths

After Floquet transformation, the terms in the space-charge potential, Eq. (6), responsible for the 6th order resonances can be expressed in terms of action-angle variables in the form

$$V_{sc,6}(J_x,J_z,\psi_x,\psi_z,\theta) \approx -\frac{1}{R}\sum_\ell |G_{60\ell}|J_x^3\cos(6\psi_x - \ell\theta + \chi_{60\ell}) - \frac{1}{R}\sum_\ell |G_{06\ell}|J_z^3\cos(6\psi_z - \ell\theta + \chi_{06\ell}) - \frac{1}{R}\sum_{\ell,\pm} |G_{4\pm2\ell}|J_x^2J_z\cos(4\psi_x \pm 2\psi_z - \ell\theta + \chi_{4\pm2\ell}) - \frac{1}{R}\sum_{\ell,\pm} |G_{2\pm4\ell}|J_xJ_z^2\cos(2\psi_x \pm 4\psi_z - \ell\theta + \chi_{2\pm4\ell}),$$

where ℓ is an integer, R is the radius of the accelerator ring, and $\theta = s/R$ is the orbiting angle in the accelerator. Here, $|G_{mn\ell}|$ and $\chi_{mn\ell}$ are the amplitude and phase of the resonance strength and they are computed by integrations around the accelerator ring:

$$\begin{aligned}
G_{60\ell} &= \frac{1}{5760\pi}\oint \frac{K_{sc}\beta_x^3(8\sigma_x^2+9\sigma_x\sigma_z+3\sigma_z^2)}{\sigma_x^5(\sigma_x+\sigma_z)^3} \\
&\quad \exp\left[j(6\phi_x - 6\nu_x\theta + \ell\theta)\right] ds, \\
G_{06\ell} &= \frac{1}{5760\pi}\oint \frac{K_{sc}\beta_z^3(8\sigma_z^2+9\sigma_x\sigma_z+3\sigma_x^2)}{\sigma_z^5(\sigma_x+\sigma_z)^3} \\
&\quad \exp\left[j(6\phi_z - 6\nu_z\theta + \ell\theta)\right] ds, \\
G_{4\pm2\ell} &= \frac{1}{384\pi}\oint \frac{K_{sc}\beta_x^2\beta_z(3\sigma_x+\sigma_z)}{\sigma_x^3\sigma_z(\sigma_x+\sigma_z)^3} \\
&\quad \exp\left\{j[4\phi_x \pm 2\phi_z - (4\nu_x \pm 2\nu_z)\theta + \ell\theta]\right\} ds, \\
G_{2\pm4\ell} &= \frac{1}{384\pi}\oint \frac{K_{sc}\beta_x\beta_z^2(\sigma_x+3\sigma_z)}{\sigma_z^3\sigma_x(\sigma_x+\sigma_z)^3} \exp\left\{j[4\phi_x \right. \\
&\quad \left. \pm 2\phi_z - (4\nu_x \pm 2\nu_z)\theta + \ell\theta]\right\} ds, \qquad (7)
\end{aligned}$$

where $\phi_{x,z} = \int_0^\theta ds/\beta_{x,z}$ are the Floquet phase advances. These strengths are essentially the ℓ-th Fourier amplitude of the integrand function. After the injection process, these resonance strength are evaluated every turn. During the resonance crossing, the emittance growth can occur, and the resonance strength can vary.

These resonant strengths depends on space charge strength and the lattice parameters of the accelerator. We can factorize the resonance strength into a factor that depends on the space charge perveance, and another dimensionless reduced resonant strengths $g_{mn\ell}$ as

$$G_{mn\ell} = g_{mn\ell}\frac{K_{sc}R}{4\epsilon_{\rm rms}^3}, \qquad (8)$$

where $\epsilon_{\rm rms} = \epsilon_{\rm N,rms}/(\beta\gamma)$ is the average of the unnormalized rms horizontal and vertical emittances. For a round beam, $K_{sc}R/(4\epsilon_{\rm rms})$ is just the linear Laslett space charge tune shift parameter, and the reduced resonance strength $g_{mn\ell}$ depends only on the lattice. In most of our study, the reduced resonance strength does not change significantly across a resonance, and the average reduced resonance strength before and after crossing a resonance is used to characterize the resonance. In fact, the reduced resonance strength is independent of the beam emittance for a round beam.

In our model, space-charge kicks are applied at the center of the focusing and defocusing quadrupoles, i.e. two kicks per superperiod. In one betatron period, there are about 8 to 12 space charge kicks depending on the betatron tunes. This may be small, however the harmonic content of these kicks are calculated according our tracking model, and the effect of the space charge kicks should depends essentially on the harmonic content, i.e. these reduced resonant strengths for the systematic resonances $6\nu_x = P$, $6\nu_z = P$, $4\nu_x + 2\nu_z = P$, and $2\nu_x + 4\nu_z = P$ are accordingly calculated by taking the Fourier integrals of the ac-

celerator lattice at the kick locations. Since the beam distribution is populated statistically, the horizontal and vertical emittances will be slightly different in different runs, these resonant strengths will be slightly different accordingly. One important feature of our model is that we can adjust the magnitudes of the reduced resonant strengths as necessary by assigning different values for the betatron functions $\beta_{x,z}$ at space-charge kick locations. In a uniform focusing accelerators, one has $\beta_{x,\mathrm{F}} = \beta_{x,\mathrm{D}} = \beta_{z,\mathrm{F}} = \beta_{z,\mathrm{D}}$, and $g_{60P} = g_{06P} = g_{42P} = g_{24P} = 0$. Note that the model employed here is independent of the radius of the accelerator ring.

This work does not include momentum width, which has small effect for large emittance beams. When momentum width is included, the separation of lattice dependency from space charge is less exact. However, the factorization of the resonance strength into the space charge and reduced resonance strength factors should remain good because $\sqrt{\beta_x \epsilon_{\mathrm{rms}}} \gg D_x \sigma_\delta$. For example, the beam parameters in Ref. [5] has $\sigma_{x\beta} = \sqrt{\beta_x \epsilon_x} \sim 8.5$ mm, and $\sigma_{x\delta} = D_x(\Delta p/p) \sim 1.6$ mm. Thus the effective horizontal rms width is $\sigma_x = \sqrt{\sigma_{x\beta}^2 + \sigma_{x\delta}^2} \sim 8.7$ mm The momentum width becomes important near the transition energy [10].

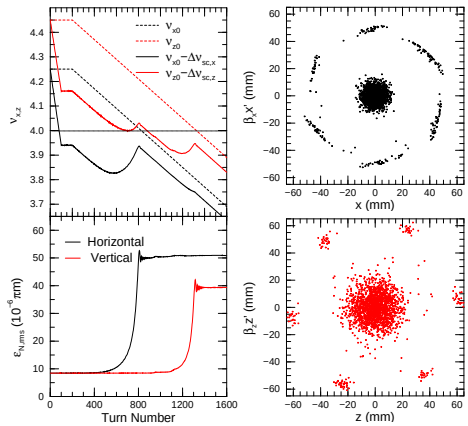

Figure 2: (Color) Top-left: After 100-turn injection at 4.0×10^{11} per turn at bunching factor $B = 2$, bare tunes are ramped downwards from $(\nu_{x0}, \nu_{z0}) = (4.25, 4.45)$ starting from turn 200 to (3.69, 3.89) at turn 1600 (ramp rate -0.0004 per turn). Systematic resonances $6\nu_{x0} = P$ and $6\nu_{z0} = P$ ($P = 24$ is the lattice periodicity) are crossed at turns 825 and 1325, respectively. Bottom-left: Emittance growths are observed when the resonances are crossed. Red and black dots are respectively the vertical and horizontal emittances. Right: Horizontal and vertical phase-space distributions at turns 820 and 1270 showing the 6th order resonances.

Tracking

Tracking has been performed with 2000 macro-particles for 1600 turns. Figure 2 shows a sample tracking with 100-turn injection of 4.0×10^{11} per turn and bunching factor $B = 2$ at bare tunes $\nu_{x0} = 4.25$ and $\nu_{z0} = 4.45$.

Starting from turn 200, the tunes are ramped downwards linearly at the rate of 0.0004 per turn until they reach 3.69 and 3.89 at turn 1600. The top-left plot shows both the bare tunes and space-charge depressed tunes as functions of turn number. We note that the horizontal tunes (black curve) of small amplitude particles has encountered $6\nu_x = P$ ($P = 24$, the lattice periodicity) resonance in the first 200 turns but show little or no emittance growtn in the bottom-left plot for the evolution of normalized rms emittances. The systematic resonances $6\nu_{x0} = 24$ and $6\nu_{z0} = 24$ are crossed at turns 825 and 1325, respectively. In the plot $\Delta\nu_{sc,x}$ and $\Delta\nu_{sc,z}$ represent the linear horizontal and vertical space-charge tune shifts. After injection and before resonances set in, the linear space charge tune shifts are $\Delta\nu_{sc,x} = 0.310$ and $\Delta\nu_{sc,z} = 0.290$. The bare horizontal and vertical tunes cross the 6th order resonances at turns 825 and 1325 respectively. The horizontal and vertical emittances start to grow about 150 turns before the corresponding resonance crossing, and level off after that. As the emittances begin to grow, the beam size increases and the linear space-charge tune shifts are reduced. The reduced resonance strengths, $|g_{60P}| = 0.00181$ and $|g_{06P}| = 0.00172$, were evaluated before the resonance crossing. The plots on the right show the particle distribution in the transverse phase spaces at turns 820 and 1270. Six islands are clearly seen in the phase space plots. Furthermore, the phase space plots indicate that the phases of g_{60P} and g_{06P} differ by π. Some decoherence is apparent for the horizontal phase space at turn 820 at the top-right plot. When crossing the 6th order resonance, particles are resonantly pushed outwards iforming 6 islands, and gradually decohere into a ring encircling the inner core. The space charge force becomes small at large distance from the center of the beam. Since we set our aperture very large at 500 πmm-mrad, no particle loss has been observed in our simulations. In a realistic accelerator with a smaller aperture, particle loss can occur.

We also note that the betatron tunes pass through two sum resonances at $4\nu_x + 2\nu_z = 24$ and $2\nu_x + 4\nu_z = 24$. The emittance growth due to these two sum resonances is smaller. Our simulations show that these sum resonances can produce about 15% of the total emittance growth at a small acceleration rate.

The reduced resonance strengths of these sum resonances for a normal lattice, where $\beta_{xF} \gg \beta_{xD}$, $\beta_{zD} \gg \beta_{zF}$, $\beta_{xF} \approx \beta_{zD}$, and $\beta_{xD} \approx \beta_{zF}$ are about 40% of those of $6\nu_x = 24$ or $6\nu_z = 24$. For a lattice with smooth betatron amlitude functions, resonance strengths of all resonances becomes small as shown in Eq. (7). If the integrands in Eq. (7) are nearly constant, their Fourier amplitudes of a nonzero harmonic is small. For example, if the integrands of the resonance strengths for $4\nu_x + 2\nu_z = 24$ and $2\nu_x + 4\nu_z = 24$ resonances are nearly constants, the kicks at the focusing quadrupole location is nearly cancelled by the kick at the defocusing location.

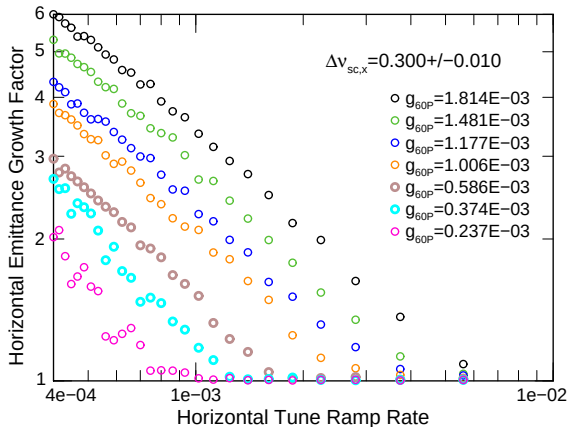

Figure 3: (Color) Horizontal emittance growth factors and across the 6th order systematic resonances $6\nu_{x0} = P$ ($P = 24$, the lattice periodicity) are plotted as functions of tune-ramp rate for various reduced resonance strengths g_{60P}. At a lower resonance strength (red circles), obtained by seting $\beta_{xF} \approx \beta_{zF}$ and $\beta_{zF} \approx \beta_{zD}$, the resonance strengths $6\nu_x = 24$ and $4\nu_x + 2\nu_z = 24$ in Eq. (7) are equal. The effect of $4\nu_x + 2\nu_z$ resonance can produce a stronger effect on the EGF, and thus shown the fluctuation in the red circle symbols.

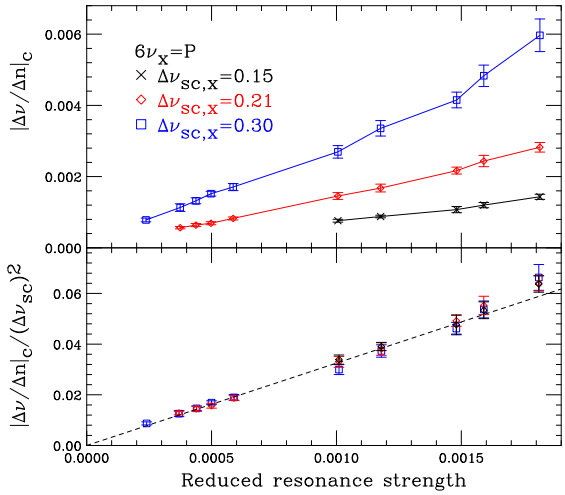

Figure 4: (Color) Top: Critical tune-ramp rates across the systematic 6th order resonance $6\nu_{x0} = P$ ($P = 24$) are plotted as functions of reduced resonance strength $|g_{60P}|$ for various linear space-charge tune shifts or bunch intensities. Bottom: The critical tune-ramp rate $|d\nu/dn|_c$ divided by $(\Delta\nu_{\rm sc})^2$ of the top plot shows scaling properties. The scaling property is shown in Eq. 9.

Scaling

The tune-ramp rate is increased gradually from $|d\nu_{x0,z0}/dn| = 0.0004$ by increasing the start-ramp-turn-number in steps of 50 in each simulation until the tune-ramp rate reaches 0.0112 with start-ramp-turn-number 1550. For each tune-ramp rate, the resonance strengths can be varied by assigning different values of betatron functions at the space-charge kicks. For example, when the betatron amplitude functions are identical at both the focusing and the defocusing quadrupole locations, the lattice is a uniform focusing model, and the space charge kicks at the focusing and defocusing locations cancel each other. Thus the space-charge resonance strengths are varied accordingly. The space-charge tune shifts, the zeroth harmonics of the space-charge kicks, are maintained constant in this resonance strength variation.

The emittance growth factor (EGF), defined as the ratio of emittances after and before the crossing of a resonance, is computed for each simulation. Equal initial horizontal and vertical emittances are assumed. The results for 100-turn injection with EGF versus tune-ramp rate for crossing the resonance $6\nu_{x0} = P$ are shown in Fig. 3.

When the EGF is larger than 1, Fig. 3 shows the power-law relationship between the EGF and the tune-ramp rate, i.e., EGF$\sim |d\nu/dn|^{-a}$ where a is a constant that may depend on the resonance strength and the space-charge tune shift. Concentrate on one of these reduced resonance strength, for example the one with $|g_{60P}| = 0.00181$, the black data points in Fig. 3. Extend the linear relationship in the log-log plot to intercept the tune-ramp rate axis at EGF$= 1$ and denote the intercept as the *critical tune-ramp rate*, which gives $|(d\nu_x/dn)_c| \approx 0.034 \pm 0.002$. At this critical tune-ramp rate, we find EGF≈ 1.1, i.e. a 10% increase in emittance, considered to be acceptable. At a 10% emittance growth, the phase space has halo surround its outer edge. At a lower resonance strength (red marks), obtained by seting $\beta_{xF} \approx \beta_{zF}$ and $\beta_{zF} \approx \beta_{zD}$, the resonance strengths $6\nu_x = 24$ and $4\nu_x + 2\nu_z = 24$ in Eq. (7) are equal. The effect of $4\nu_x + 2\nu_z$ resonance can produce a stronger effect on the EGF, and thus shown the fluctuation in the red circle symbols. Nevertheless, the trends of EGF vs $|d\nu/dn|$ is similar.

The critical tune-ramp rate is computed in the same way for all data belonging to each resonance strength. We find that for linear space-charge tune shift $\Delta\nu_{sc,x} = 0.300$, the power in the power law assumes the value $a = 0.66$ at $|g_{60P}| = 0.00181$ and increases to $a = 1.03$ as the resonance strength decreases to 0.00024. The increase in the slope due to may have resulted from the combination of $6\nu_x = 24$ and $4\nu_x + 2\nu_z = 24$ resonances.

Similar computations are carried out for different beam intensities: 70-turn injection with bunch intensity $N_{\rm B} = 33.3 \times 10^{10}$ with $\Delta\nu_{sc,x} = 0.212$, $\Delta\nu_{sc,z} = 0.211$, and 50-turn injection with bunch intensity $N_{\rm B} = 23.8 \times 10^{10}$ with $\Delta\nu_{sc,x} = 0.153$, $\Delta\nu_{sc,z} = 0.152$. Power law relationships are also evident at these bunch intensities when the EGFs are slightly larger than unity. The critical tune-ramp rates are computed and plotted in the top plot of Fig. 4, where the error bar in arises mostly from the uncertainty in straight line-fitting of the power law and the uncertainty in the intercept on the tune-ramp rate $|d\nu/dn|$ axis in Fig. 3. The lines in the top plot are drawn to guide the eyes.

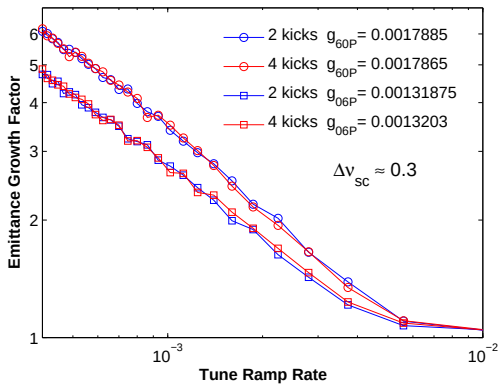

Figure 5: (Color) Comparison of the Emittance growth factors for 2-kicks and 4-kicks in each FODO cell for two 6th order resonances. Note that increasing the number of kicks does not change the EGF.

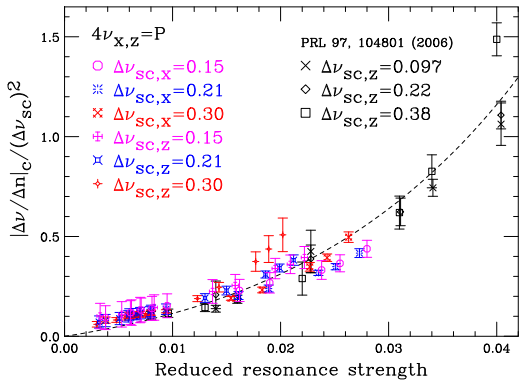

Figure 6: (color) The critical tune-ramp rate versus strength g_{04P} of 4th order resonance $4\nu_{z0} = 24$ of Refs. [6] and [7] is expressed in $|d\nu/dn|_c/(\Delta\nu_{sc})^2$ vs the reduced resonance strengths. The dashed line is a curve fit of $8.4\ g_{04P}\ \exp(31 g_{04P})$. it appears that $|d\nu/dn|_c$ appears to be larger than the fitted curve at smaller resonance strengths. At this moment, we do not have explanation.

The space charge resonance strengths are proportional to $\Delta\nu_{\rm sc}$, and the number of turn that the beam is under the influence of the resonance is $\Delta n \approx \Delta\nu_{\rm sc}/|d\nu/dn|$. Thus the EGF should be proportional to $(\Delta\nu_{\rm sc})^2/|d\nu/dn|$. The scaled critical tune-ramp rate, defined as $|d\nu/dn|_c/(\Delta\nu_{\rm sc})^2$, is plotted at the bottom of Fig. 4 vs the reduced resonance strength. The scaling works very well indeed. It seems that the critical tune-ramp rate can be fitted by

$$\left|\frac{d\nu}{dn}\right|_c \approx 65\ g_{60P}\ (\Delta\nu_{\rm sc})^2, \qquad (9)$$

shown as the dashed line in the bottom plot of Fig. 4. The critical tune-ramp rate can easily be obtained once the bunch intensity and 6th order resonance strengths are given. These plots provide a guideline for the design of FFAGs in order to avoid excessive emittance growths during the crossing of the systematic 6th order resonances.

Four kicks per FODO cells

We also carry out calculation with 4-kicks per FODO cell to check the validity of our argument that the emittance growth is determined by essentially the resonance strength. Figure 5 shows that the emittance growth factors for 4 kicks and 2 kicks per FODO cell depends essentially on the resonance strength. Increasing the number of kicks in each FODO cell does not affect the emittance growth factor.

Comparison with the 4th order systematic resonances

The approximate space charge forces used in the simulations of Ref.[6, 7] roll off too rapidly at large distance from the center as shown in the Appendix of Ref.[7]. Since emittance growth occurs mainly for large amplitude particles, we would like to use our exact space charge force to re-evaluate the EGF and deduce the critical tune-ramp rate vs the resonance strength. Figure 6 shows the scaled critical tune-ramp rate, $|d\nu/dn|_c/(\Delta\nu_{\rm sc})^2$, vs the reduced resonance strength in red, blue and magenta colors for the $4\nu_x = P$ and $4\nu_z = P$ resonances.

In order to compare with our earlier results, we multiply the scaled critical tune-ramp rate of Ref. [6, 7] by a factor of 2 and plot the results in Fig. 6. This means that a sharper roll-off in the approximate space charge force under-estimate the critical tune-ramp rate by a factor of 2. However, the scaling properties is still maintained. An approximate curve fit of the 4th order resonance critical tune-ramp rate, shown as the dashed line in Fig. 6, is

$$\left|\frac{d\nu}{dn}\right|_c \approx 8.4\ (\Delta\nu_{\rm sc})^2\ g_{04P}\ \exp\{31 g_{04P}\}. \qquad (10)$$

When g is small, the scaling law is linear. The scaling laws of Eqs. (9) and (10) can be understood understood as follows. First the effect systematic resonance strength is proportional to $g \cdot |\Delta\nu_{\rm sc}|$, where g is the reduced width. Second, the number of turn to pass through a resonance is $|\Delta\nu_{\rm sc}/(d\nu/dn)|$. The scaling laws indicate that the number of turns to pass through a resonance for getting the same EGF is nearly constant for each resonance. The exponential dependence of Eq. (10) awaits for explanation.

FOURTH ORDER PARAMETRIC RESONANCES

Octupoles are often necessary to provide betatron tune spreads for the Landau damping of unwanted transverse instabilities. These octupoles are specially placed in the accelerator ring to maximize tune spreads and minimize nonlinear effects. As a result, the periodicity of the ring will be broken. Another source of octupole field comes from random nonlinear errors in lattice magnets. They break the

periodicity of the ring also. We add a single octupole in our model accelerator ring at the D-magnet of the last period.

Resonance Strengths

The potential of the octupole fields is

$$V_4(x,z) = -\frac{1}{4!}\frac{B_3}{B\rho}\left(x^4 - 6x^2z^2 + z^4\right), \qquad (11)$$

where $B_3 = \partial^3 B_z/\partial x^3$. After Floquet transformation, the terms responsible for the 4th order resonances can be expressed in terms of action-angle variables in the form

$$V_4(J_x, J_z, \psi_x, \psi_z, \theta) \approx -\frac{1}{R}\sum_\ell |G_{40\ell}| J_x^2 \cos(4\psi_x - \ell\theta + \chi_{40\ell}) - \frac{1}{R}\sum_\ell |G_{04\ell}| J_z^2 \cos(4\psi_z - \ell\theta + \chi_{04\ell}) - \frac{1}{R}\sum_{\ell,\pm} |G_{2\pm2\ell}| J_x J_z \cos(2\psi_x \pm 2\psi_z - \ell\theta + \chi_{2\pm2\ell}), \qquad (12)$$

where ℓ denotes any integer. In above $|G_{mn\ell}|$ and $\chi_{mn\ell}$ are the amplitude and phase of the resonance strength and they are computed by integrations around the accelerator ring over all the octupole fields:

$$G_{40\ell} = \frac{1}{96\pi}\oint \frac{B_3\beta_x^2}{B\rho}\exp\left[j(4\phi_x - 4\nu_x\theta + \ell\theta)\right]ds,$$
$$G_{04\ell} = \frac{1}{96\pi}\oint \frac{B_3\beta_z^2}{B\rho}\exp\left[j(4\phi_z - 4\nu_z\theta + \ell\theta)\right]ds,$$
$$G_{2\pm2\ell} = -\frac{1}{16\pi}\oint \frac{B_3\beta_x\beta_z}{B\rho}\exp\left\{j\left[2\phi_x \pm \phi_z - (2\nu_x \pm 2\nu_z)\theta + \ell\theta\right]\right\}ds. \qquad (13)$$

These resonance strengths can be made dimensionless by introducing the reduced resonance strengths

$$g_{mn\ell} = G_{mn\ell}\epsilon_{\rm rms} \qquad (14)$$

where $\epsilon_{\rm rms}$ is the rms emittance of the beam. Across a thin octupole of length Δs, the change in horizontal and vertical divergences are given by

$$\Delta x' = \tfrac{1}{6}S_4(x^3 - 3xz^2),$$
$$\Delta z' = \tfrac{1}{6}S_4(z^3 - 3x^2z), \qquad (15)$$

where the octupole strength is defined as $S_4 = B_3\Delta s/B\rho$ and Δs is the length of the octupole. For our test beam that has a kinetic energy of 1 GeV, $S_4 = 50\ \mathrm{m}^{-3}$ corresponds to a pole tip field of 0.035 T if the octupole physical aperture is of radius 5 cm and length 1 m. With the octupole placed at a defocusing quadrupole location with $\beta_x = 6.3$ m, $\beta_z = 21.4$ m, the resonance strengths at $\epsilon_{\rm rms} = 4.61\times10^{-6}$ πm (normalized 95% emittance $\epsilon_{\rm N} = 50\times10^{-6}$ πm) are $|g_{40\ell}| = 3.03\times10^{-5}$, $|g_{04\ell}| = 3.50\times10^{-4}$, $|g_{2\pm2\ell}| = 1.03\times10^{-4}$. Since $|g_{40\ell}|$ is much smaller than $|g_{04\ell}|$ we study the emittance growth in passing through $4\nu_z = \ell$ resonance. It is difficult to study the sum resonance for emittance growth, because they can cause particle loss. We can easily avoid the difference resonance $2\nu_x - 2\nu_z = \ell$. Only the resonance $4\nu_{z0} = \ell$ will be studied here.

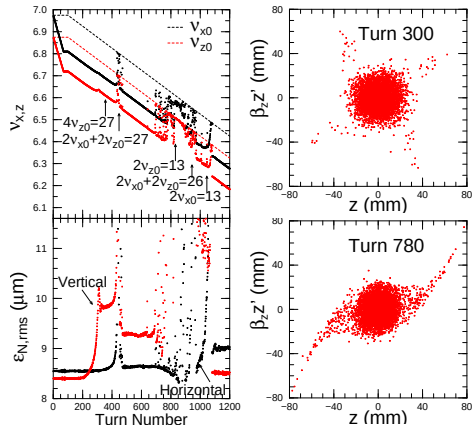

Figure 7: (Color) Top-left: The bare tunes (dashed lines) and the tunes depressed by linear space charge (thick dots) vs the turn number for a beam with 70-turn injection at 3×10^{11} per turn. The linear space charge tune shift parameters are $(\Delta\nu_{\rm sc,x}, \Delta\nu_{\rm sc,z}) = (0.167, 0.165)$. The bare tunes are ramped downwards from $(\nu_{x0}, \nu_{z0}) = (6.975, 6.875)$ at turn 100 at the rate of $|d\nu_{x0,z0}/dn| = 0.0005$. Octupole driven parametric resonances $4\nu_{z0} = 27$ and $2\nu_{x0} + 2\nu_{z0} = 27$ are crossed at turns 350 and 450, respectively. Either half-integer resonance $2\nu_{z0} = 13$ or a fourth order resonance $4\nu_{z0} = 26$ is crossed in the vertical plane at turn 850. Bottom-left: Emittance growths are observed when the resonances are crossed. Heavy beam loss is also observed to correlate the emittance reduction. Right: vertical phase-space distributions at turn 300 (top) and 780 (bottom), demonstrating the crossing of $4\nu_{z0} = 27$ and $2\nu_{z0} = 13$, respectively.

Tracking

Because particle motion is much more sensitive to external magnetic field near a resonance, our tracking is performed with 5000 macro-particles for 1200 turns. A larger number of macro-particles are used here because a smaller number of macro-particles is more sensitive to the loss and action increment of a few particles. This can lead to spurious emittance growth. Figure 7 shows a sample tracking with 70-turn injection of 3×10^{11} protons each at bare tunes $\nu_{x0} = 6.975$ and $\nu_{z0} = 6.875$.

Starting from turn 100, both tunes were ramped downward linearly at the rate of 0.0005 per turn. The top-left plot shows both the bare tunes (dashes) and the space-charge depressed tunes (thick dots) as functions of turn number, while the bottom-left plot show the evolution of normalized rms emittances. The octupole strength was $S_4 = 20\ \mathrm{m}^{-3}$. There is a vertical emittance growth near the $4\nu_{z0} = 27$ resonance at turn 350. This is verified by the vertical phase space plot (of turn 300) at the top-right with the four arm-like structure. When the betatron tunes move downward, the beam particles encounters the resonance tori. Large amplitude particles are squeezed along the resonance sep-

aratrix outward to a large amplitude. The reduction of the vertical emittance at the bottom-left plot of Fig. 7 after the passing of the $4\nu_{z0} = 27$ resonance arises from the particle loss.

The next resonance encountered is the $2\nu_{x0}+2\nu_{z0} = 27$ sum resonance at turn 450. Then the vertical hits the half-integer resonance $2\nu_{z0} = 13$ at turn 800, which is verified by the vertical phase space plot (of turn 780) at the bottom right, where we see particles streaming out in two directions. However, the half-integer stopband driven by the octupoles is much weaker than that driven by the random quadrupole errors. There is another 4th order sum resonance $2\nu_{x0} + 2\nu_{z0} = 26$ at turn 950 followed by another half-integer resonance $2\nu_{x0} = 13$ at turn 1050. The 4th order resonance in the horizontal plane $4\nu_{x0} = 27$ should occur near turn 550, but it has almost been invisible, probably a result of the small horizontal betatron function at the octupole location ($\beta_{x,D} = 6.3$ m vs $\beta_{z,D} = 21.4$ m).

Note that the resonances crossed and the emittance growths always occur some revolution turns before the turn numbers suggested by the bare tunes. For example, $4\nu_{z0} = 27$ predicts a resonance at turn 350, but the actual emittance growth peaks some 30 turns before that. The shifting of the resonance position comes from the depressed tunes of the space-charge force. Figure 7 shows that the resonance position of a lower order resonance will be more determined by the space charge depressed tunes. The references of Fig. 7 by the bare tunes are intended to where the effect of a resonance occurs.

Unlike the resonances driven by the space charge force, beam loss of 6.2% occurs during the 1200-turn tracking. The space charge force decreases when the actions of a particle are larger than $3\sigma_{x,z}$. On the other hand, the perturbing force increases with amplitudes for nonlinear magnetic fields. In the simulation, when the action exceeds a certain pre-determined value, the particle is defined as lost and is removed from the simulation. The computation of emittances might become inaccurate in the presence of particle loss. Particles outside a core are pushed outward by the nonlinear force and become lost leaving behind a core that might have emittances that are rather small. This explains why emittances appear to decrease in the emittance plot in Fig. 7 after passing a resonance. We will include only those simulations where no particle loss is recorded across the resonance for the emittance growth. Thus we cannot study simulations with octupole strength larger than $S_4 \approx 50$ m^{-3}, and we will study the scaling property of the 4th order parametric resonance $4\nu_z = \ell$ resonances. Our results should be applicable to $4\nu_x = \ell$ resonance as well.

There are three parameters in the study of emittance growth crossing the octupole driven resonance $4\nu_{z0} = 27$: the beam intensity, the octupole strength, and the tune-ramp rate. For the beam intensity, we study simulations of 70-turn injection with 1×10^{11}, 2×10^{11}, 3×10^{11}, and 4×10^{11} protons per turns. They correspond to bunch intensity 8.33×10^{10}, 16.7×10^{10}, 25.0×10^{10}, and 33.3×10^{10}. The bunching factor and the beam kinetic energy have always been chosen to be $B = 2$ and 1 GeV. At the normalized 95% emittances of 50×10^{-6} πm, the corresponding linear space-charge tune shifts are $(\Delta\nu_{sc,x}, \Delta\nu_{sc,z}) =$ (0.056, 0.052), (0.112, 0.103), (0.167, 0.165), and (0.223, 0.207), respectively. The octupole strength is varied from $S_4 = 10$ m^{-3} to 50 m^{-3}. The tune-ramp rate is varied from $|d\nu/dn| = 0.00003$ to 0.006.

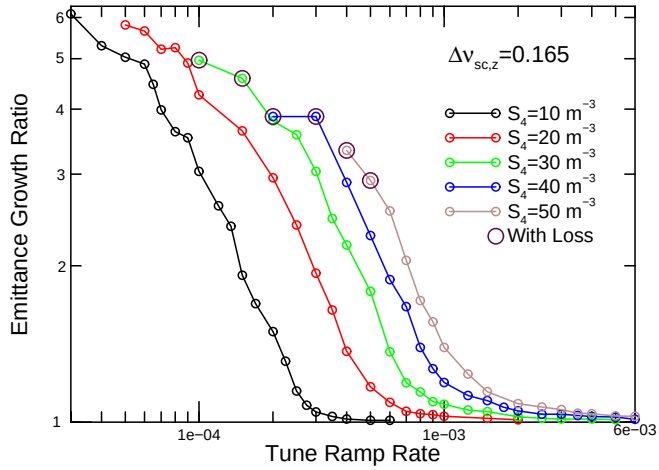

Figure 8: (Color) Emittance growth factors across the 4th order resonances $4\nu_{x0} = 27$ driven by an octupole in the presence of space charge as functions of tune-ramp rate for various octupole strengths. Data encircled involve particle loss and are discarded in the critical tune-ramp-rate analysis.

Scaling

The results for a sample of simulations with $\Delta\nu_{\rm sc} = 0.165$ are shown in Fig. 8 as log-log plots. Similar to the systematic resonances discussed above, we observe linear relationship between the EGF and tune-ramp rate for each reduced resonance strength when the EGF is slightly larger than unity. The EGF saturates at smaller tune-ramp rates due either to beam loss or the limited the resonance islands in phase space area for small octupole magnetic field. When the betatron tunes move downward, the resonance islands move inward in phase space and sqeeze particles outward in phase space. When the betatron tunes are lower than the resonance line $4\nu = \ell$, resonance islands disappear for $S_4 > 0$ cases.

When the EGF is less than 3, the power law is still nearly valid, i.e. EGF$\sim |d\nu/dn|^{-a}$, where $a \sim 0.8$ to 1.0 depends slightly on the resonance strength and the space-charge tune shift. We draw a straight line in the EGF vs $|d\nu/dn|$ log-log plot in the power law regime, and the line cuts the $|d\nu_z/dn|$-axis to obtain the critical tune-ramp rate. In general at these critical tune-ramp rates, the EFG is less than 1.2. For each bunch intensity, the critical tune-ramp rate is plotted in Fig 9 as a function of the resonance strength $|g_{04\ell}|$. The error bars reflect the uncertainty of the linear lines of the plots and their intercepts on the $|d\nu_z/dn|$-axis.

The number of turns that the beam is under the influence

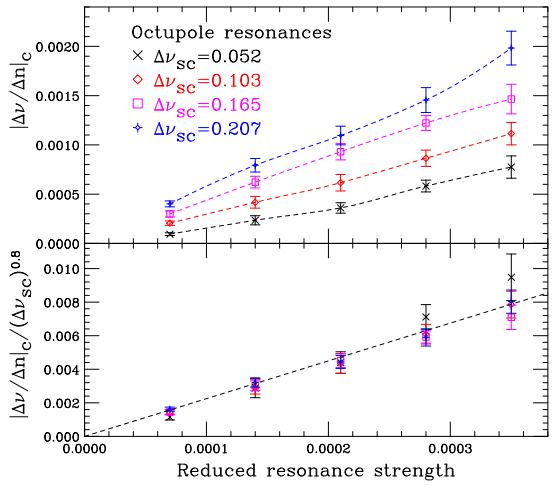

Figure 9: (Color) Top: Critical tune-ramp rates across the octupole driven 4th order resonances $4\nu_{z0} = 27$ are plotted as functions of reduced resonance strength $g_{04\ell}$ for various bunch intensities. Dashed lines are drawn to guide the eyes. Bottom: $|d\nu/dn|_c/(\Delta\nu_{\rm sc})^{0.8}$ for the octupole driven 4th order resonances $4\nu_{z0} = 27$ vs the reduced resonance strength $g_{04\ell}$. The dashed line is a linear fit to the data.

of the resonance is approximately $\Delta n \sim \Delta\nu_{\rm sc}/|d\nu/dn|$. Thus the EGF is proportional to $\Delta\nu_{\rm sc}/|d\nu/dn|$, and thus we expect $|d\nu/dn|_c \sim \Delta\nu_{\rm sc}$. We find that the critical tune-ramp rate divided by $(\Delta\nu_{\rm sc})^{0.8}$ gives a good scaling property for the four simulation-data sets, shown at the bottom of Fig. 9. The dashed line in the bottom plot of Fig. 9 is

$$\left|\frac{d\nu}{dn}\right|_c \approx 23\, g_{40\ell}\, (\Delta\nu_{\rm sc})^{0.8}, \qquad (16)$$

which is approximately 2.6 times more stringent than that of the fourth order space charge resonances as shown in Eq. (10). Figure 9 provides useful guidelines for the tolerable octupolar resonances in accelerators that their betatron tunes must pass through the fourth order resonances. For a given linear space-charge tune shift of the beam and given random octupole strengths, the minimum rate of crossing the 4th order resonance can be determined for a tolerable emittance growth.

Particle trapping in islands and Beam loss

Since we study only tune ramp downward, the sign of octupole resonance strength plays an important role in resonance growth and beam loss. The 4th order resonances occurs only in one direction in the betatron tune space. In our study with $S_4 > 0$, the resonance condition can only exist at $\nu_z - \ell/4 \geq 0$. As the betatron tune is ramp downward, large amplitude particles encounter the tori of resonance and the separatrix of the 4th order resonance sqeezes particles out to a large amplitude. As the tune is further ramp downward, these islands move inward and get smaller in size. Once the bare tune passes $4\nu_0 = \ell$, the phase space is resonance free. Unless the resonance strength is large, beam loss is unlikely, and the emittance growth is limited as shown in Fig. 8.

On the other hand, if the sign of the resonance strength $G_{04\ell}$ is changed, the resonance condition exists only at $\nu_z - \ell/4 \leq 0$. As the betatron tune is ramped down, resonance occurs at $\nu_z = \ell/4$ at the center of the bunch (the space charge tune shift can change this picture slightly). As the tune is ramped further downward, the islands move outward, increase in size, and trap particles with it. These trapped particles will eventually be lost at the dynamic aperture [12].

CONCLUSIONS

For a non-scaling FFAG, the beam motion may cross many betatron resonances. In this paper, we improve our simulation model by using the space charge potential for Gaussian-beam without round beam approximation. We then performed simulations to study emittance growths on crossing the systematic 6th order resonances driven by the space-charge force. Just as in the investigation in Refs. [6] and [7], we find power law works between the EGFs and tune-ramp rates for the 6th order resonance $6\nu_{x0} = P$. A critical tune-ramp rate is thus determined by EGF curve cutting the tune-ramp rate axis. At the critical tune-ramp rate, the emittance growth is typically less than 10%. The critical tune-ramp rate vs the space-charge tune shift and the reduced resonance strength shows a simple scaling property given by Eq. (9). A similar scaling law also exists for the 4th order systematic space charge resonances. The scaling law can serve as a design guide for non-scaling FFAGs so that emittance growths across these resonances can be kept within toleration.

For a lattice similar to that of the Fermilab Booster with a linear space-charge tune shifts of ~ 0.30, the critical tune-ramp rates is $d\nu/dn \sim 0.006$ per turn. This means that, when the particle kinetic energy is 1 GeV and the betatron tune is 4, the energy gain per revolution should be of the order of 2.2 MeV, which is rather large for the low frequency rf systems. For this reason, phase advance per cell should not hit $\frac{\pi}{2}$ for the 4th order systematic resonance and not cross $\frac{\pi}{3}$ for the 6th order systematic resonance during the FFAG ramp cycle. The 6th order resonances are intrinsically weaker than the 4th, e.g., the maximum reduced strengths of g_{60P} and g_{06P} are typically less than 1/20 of the maximum g_{40P} and g_{04P} shown in Fig. 6, the critical tune-ramp rate is smaller as shown in Fig. 4. However, the minimum tune-ramp rate may still be challenging in the FFAG proton driver design.

For the parametric 4th order resonance $4\nu_{z0} = \ell$, we also find linear scaling relations in the log-log plot of EGF versus tune-ramp rate. High intensity beams are severely limited by nonlinear resonances driven by external magnetic field errors. These resonances can cause beam loss. For example, if the reduced resonance strength the parametric 4th resonance is $|g_{04\ell}| \leq 3.5 \times 10^{-4}$, which is a relatively large number, and the linear space-charge tune

shift is $\Delta\nu_{sc,z} = 0.25$, then the corresponding critical tune-ramp rate should be about $\sim 2 \times 10^{-3}$ per turn in order to limit emittance growth. In fact, since the tune ramp rate for the FFAG is always downward, the sign of $g_{04\ell}$ or $g_{40\ell}$ is very important. All parametric resonances with detuning depends on the signs of detuning parameter and the resonance strength [11]. If the resonance occurs in the range $\nu - \frac{1}{4}\ell > 0$ and betatron tune is ramped downward, emittance will grow but the resonance islands are moving inward to the center of the beam, and they disappear after passing through the resonance. However, if the resonance occurs in the range of $\nu - \frac{1}{4}\ell < 0$ and betatron tune is ramped downward, the resonance islands move outward in action, and the beam particles are trapped in resonance islands and can be extracted. Since the parametric resonances driven by error magnetic fields can cause beam loss, stopband correction must be implemented in order to minimize beam loss and emittance growth. It would be interesting to carry out experimental measurements of EGF for various resonances driven by the space charge potential and magnet errors. Experimental results can be used to verify our scaling law and provide design-guidelines for future high power accelerators.

REFERENCES

[1] E. D. Courant, M. S. Livingston, and H. S. Snyder Phys. Rev. **88**, 1190 (1952)

[2] K. R. Symon, D. W. Kerst, L. W. Jones, L. J. Laslett, and K. M. Terwilliger, *Fixed-Field Alternating-Gradient Particle Accelerators*, Phys. Rev. **103**, 1837 (1956).

[3] M. Aiba *et al.*, Proc. of 2002 European Particle Accelerator Conference, Paris, p. 1028 (2002).

[4] C. Johnstone, W. Wan, and A. Garren, Proc. 1999 Particle Accelerator Conference, New York, p. 3068 (1999).

[5] A.G. Ruggiero, Brookhaven Report C-A/AP/#219, 2005.

[6] S.Y. Lee, Phys. Rev. Lett. **97**, 104801 (2006).

[7] S.Y. Lee, G. Franchetti, I. Hofmann, F. Wang, and L. Yang, New J. Phys. **8**, 291 (2006).

[8] A. Chao and M. Month, Nucl. Instru. and Methods, **121**,129 (1974); M. Aiba and S. Machida, Proc. of the European Particle Accelerator Conf. 2004, p. 2119 (EPAC, 2004).

[9] S. Y. Lee, *Accelerator Physics*, 2nd edition (World Scientific, Singapore, 2004).

[10] Xiaobiao Huang, S.Y. Lee, K.Y. Ng, and Y. Su, PHYS. REV. SPECIAL TOPICS - ACCELERATORS AND BEAMS **9**, 014202 (2006).

[11] M. Ellison *et al.*, AIP Conference Proceedings #**292**, p. 170 (1992).

[12] R. Cappi and M. Giovannozzi, Phys. Rev. Lett. **88**, 104801 (2002).